

Chapter 2

The Lithosphere Extension and Hydrocarbon Generation in the Eastern Continental Passive Margin of India

Abstract The chapter analyzes the changes in the tectonic and thermal evolution of the lithosphere in the transition from shallow to deep-water shelf for the example of passive continental margin of India in the Bay of Bengal. The study bases on numerical reconstructions thermal evolution of 10 sedimentary sections, five of which locate within shallow offshore with water depth of 10–90 m and five others in the deep offshore with water depth of 1900–2800 m. The difference in the amplitude of the crust thinning, thermal and maturation conditions of the main sedimentary formations of sedimentary sections in shallow and deep-water offshore are discussed in detail. The consequences of these differences in the generation of different fractions of hydrocarbons by probable source rocks of the basin are considered also.

Keywords Passive margin • Bay of Bengal • Tectonic subsidence • Lithosphere extension • Maturity level • Hydrocarbon generation • Thermal activation of basin

2.1 Geological History of the Krishna-Godavari and Mahanadi Basins

2.1.1 *Tectonic History of the Bay of Bengal*

The eastern seaboard of India is a rifted divergent margin that evolved since Late Jurassic related to the break up and drifting of Indian and Antarctic plates during the breakup of eastern Gondwanaland [1–3]. The margin is geomorphologically and tectonically segmented by major faults and Visakhapatnam, Nayudupeta and Chingleput highs into the Bengal, Mahanadi, Krishna-Godavari, Palar and Cauvery Basins [4]. At the same time two great part of the margin are considered: a rifted northern part and southern sheared (transformed) part. Whereas the rifted northern part, including the Bengal, Mahanadi and Krishna-Godavari seaboard is characterized by sedimentary basins having coast parallel horst-graben structures,

the Cauvery basin along the sheared segment shows development of pull-apart basins and intervening ridges oblique to the N-S shore-line [1].

In the pre-break up reconstructions of Gondwanaland, Enderby Land and Mac Robertson Land of Antarctica are placed against east coast of India [4, 5]. Evolution of sedimentary basins in the eastern passive margin of India started in the Permian-Triassic with the stage of early rifting, formation of system of aulacogens along the Mahanady, Godavary, Krishna and Cavery rivers which flow along the dead branches of R-R-R triple junctions [1, 2, 6]. These aulacogens are aligned in a NE-SW trend (or in a NNE-SSW trend in the south), parallel to the Eastern Ghats of Precambrian age. During the Jurassic, rifting continued with formation of a set of rift triple junctions. Graben subsidence and its infill by sediments continued, block faulting was still active. The Godavari and Mahanadi grabens had continuity with the rift-like structures in the Enderby Land and the Lambert rift, respectively [7].

Cauvery Basin was initiated in the Late Jurassic, in response to development of Natal Basin between Africa-India (with Madagascar)-Antarctica at the rift propagating from the South. This crustal extension resulted in counter clockwise movement of Sri Lanka [4]. During Late Jurassic-Early Cretaceous (Kimmeridgian-Valenginian) the west Australia-India rift propagated further to the North-West. This extension was oblique and resulted in formation of horsts (Bapatla, Tanaku, Yanam horsts) and grabens (Krishna, West Godavari and the East Godavari sub-basins) in the Krishna-Godavari Basin [4]. The major Godavari rift extends both onland and offshore. On land, it is exposed near Wardha towards the north-western direction and extends to the sea in the south-east direction [8]. In the seaward portion, it crosses the shelf and enters the deep sea. The basin is dominated by deltaic plains near the sea-land boundary. Development of Mahanadi Basin was also initiated during this period. Mailaram high (rift shoulder) delivered sediments into the newly formed grabens/basins [4]. The three failed arms of the R-R-R triple junctions are Bengal-Purnea, Mahanadi-Hasdo and Lambert grabens, while along the two other arms (Bengal-Bangladesh-Assam and Krishna-Godavari-Mahanadi arms) rifting progressed and led to separation [4].

The oblique extension of the India and west Australia rift up to Krishna-Godavari Basin in the Early Cretaceous (Barriasian-Hauterivian) followed by asymmetric seafloor spreading [9], resulted in a transpression along the junction between Antarctica and Sri Lanka-India. This led to development of a NNW-SSE trending transcurrent fault along which Antarctica moved southward. The angular unconformity within synrift sediments in the Penar area of the Krishna-Godavari Basin marking beginning of mobilization is considered as the period of initiation of transcurrent movement between India and Antarctica. Ramana et al. [9] have identified magnetic anomaly of the Mesozoic crust to be 133–118 Ma old in the Bay of Bengal. As a whole, the breakup of India and east Antarctica could not be older than M0 whereas most of the oceanic crust in the Bay of Bengal evolved during the Cretaceous Normal Superchron (120–84 My; [10]).

Syntectonic infill of the aulacogens and main rift arms by sediments continued in Early Cretaceous. The latter culminates in seafloor spreading between India and Australia-Antarctica as Eastern Gondwana broke up about 140–125 Ma. It appears that the relative timing of crustal extension initially was earlier in the northern part than in the southern part and also the magnitude of extension was more in north than in south [6]. As a whole, splitting of eastern Gondwana in Upper Jurassic-Lower Cretaceous can be divided into two stages [3]. The first break-up occurred with separation of Greater India from Australia and East Antarctica during the Early Cretaceous [11]. Additional thinning of the crust assumedly along the Kakinada Trough, which is a half-graben parallel to the coast [12], subsequently became a favorable breakup zone, which occurred because of a northward ridge jump [13] and resulted in the separation of the Elan Bank from India at M2. The crust thinning is confirmed by the gravity-derived crustal models. They indicate that the crust at the eastern Indian shield margin is 39–41 km thick and thins to as much as 20–23 km at the Ocean Continent Transition (OCT). In addition, there are several structural highs within the offshore that could be a continental fragment left behind during the breakup between India and the Elan Bank [14].

In the second stage of the splitting, micro-continent of Elan Bank, which presently lies on the western margin of the Kerguelen Plateau, got detached from the eastern margin of India at about 120 Ma (Fig. 2.1; [13, 14]). Therefore, the most part of the oceanic crust in the Bay of Bengal was formed during the Cretaceous Magnetic quiet period (120–84 Ma) that explains the lack of pronounced magnetic anomaly in the Bay of Bengal [3]. In the Late Cretaceous, the Crozet hotspot had emplaced the 85° E Ridge and some isolated structural highs on oceanic crust that was already formed during the Cretaceous quiet period. The 85° E Ridge has begun its formation about 85 My ago in the northern Bay of Bengal on the oceanic crust of about 35 My old [3, 16].

In the Middle and Later Cretaceous, early drift, volcanic activity, drainage of aulacogens along the Mahanadi and Godavari rivers toward the East continued. Sea floor spreading and subduction of the Tethyan Ocean beneath southern Tibet continued forcing the Indian plate northwards towards Eurasia. The spreading rate of Indian Ocean floor increased further from 84 Ma onwards and reached maximal value about 66–64 Ma [2, 6, 14]. At the end of Cretaceous, when the rifting ceased, some parts of the basins were risen above sea level and underwent by erosion.

In the Early Paleocene, the first soft collision took place as continental India collided with the Eurasian continental margin. Rifting has ceased and India was drifting northwards. In the Middle Eocene, the hard collision took place as continental India collided with continental Eurasia. In Oligocene, a slightly northern shift of direction occurred as continental India also collided with the Indochina plate. In the Early Miocene, continuing shift of India to the North led to rise of the Himalayas to the extent when deposition of sediments of the Ganges began to affect the sedimentation of all the eastern coast of India [1, 4].

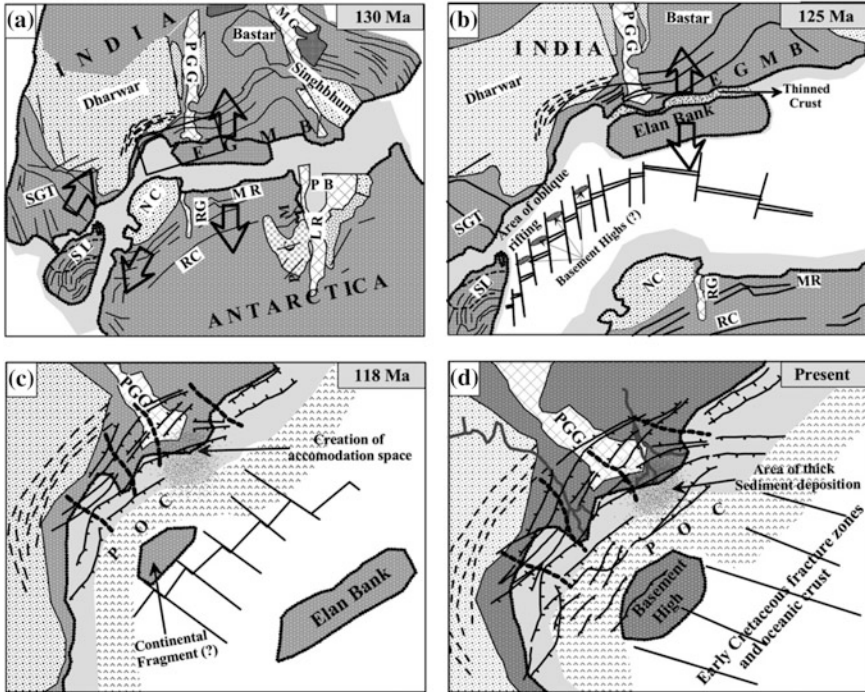


Fig. 2.1 Schematic representations of the rifting history and the double breakup events between the East Coast of India, Elan Bank and the Eastern Antarctica, and the development of the Krishna-Godavari (K-G) basin (after [14]). **a** Pre-breakup scenario just before M9 (130 Ma) showing the sense of future breakup. Area shown in rectangle is already under subsided condition, due to the pre-existing NW-SE trending Pranhitae-Godavari Graben (PGG) and NE-SW trending Jurassic rift systems developed along the coast. **b** Breakup of East Antarctica with the southern part of East Coast of India led to the development of oblique fracture zone trends and generation of late Mesozoic (younger to M4) crust at the margin. Formation of basement highs during the early breakup is indicated as inferred by Krishna et al. [15]. Significant thinning of the crust took place during this time between India and the Elan Bank. **c** Ridge jump at M2 gave rise to splitting of Elan Bank from India. Instabilities in spreading segments caused a small portion of the Elan Bank to be left behind with the Indian plate. K-G Basin was taking shape, the coastal cross trends helped to further segment the basin. The two cross trends along the PGG created a major accommodation space in the Godavari offshore. **d** The K-G Basin with its present geological features. SGT Southern Granulite Terrain, EGMB Eastern Ghat Mobile Belt, MG Mahanadi Graben, MR Mac. Robertson Land, PB Prydz Bay, LR Lambert Rift, RG Robert Glacier, NC Napier Complex, RC Rayner Complex, PCM Prince Charles Mountains

2.1.2 Sedimentation History

The sediments of the Pre-Break stage are absent in the basins of the East Coast of India except of deepest local areas of grabens [4]. Therefore, we begin the discussion of sedimentary blanket of the region with syn-rift sediments. As a whole,

the East Coast sedimentary supergroup of the eastern passive margin of India can be subdivided into two major tectono-stratigraphic sequences: (1) Late Jurassic-Early Cretaceous syn-rift megasequence, comprised largely of non-marine units, overlain by (2) Early Cretaceous (Aptian)—Cenozoic post-rift megasequence, comprised of marine sedimentary formations [2, 6]. The thickness of syn-rift sediments is controlled by the structural geometry, which in these basins is characterized by a series of NE-SW trending horsts and grabens, while post-rift sediments show an overall thickening seawards.

The syn-rift sedimentary infill is essentially fluvial and lacustrine (Fig. 2.2). Sedimentary sequences of Aptian-Albian age (Andaman and Palk Bay formations) belong also to sin-rift deposits). They were coarse sand eroded from the higher horst block and deposited in the intervening lows. Mailaram High (rift shoulder) initiated about 144 Ma [17] delivered sediments into the newly formed grabens/basins of the Krishna-Godavari and Mahanadi Basins. During Late Jurassic-Early Cretaceous (Kimmeridgian-Valenginian), deposition of *Nellore claystone*, *Krishna Formation and Pennar shale* took place in Krishna-Godavari Basin and deposition of Athgarh sandstone—in Mahanadi Basin [4]. As result of uplift of Nellore high, *Nellore claystone*, *Bapatla sandstone and Pennar shale* were deposited in the southern part of Krishna-Godavari Basin, while in Kakinada Bay area, the *Golapalli sandstones* were deposited.

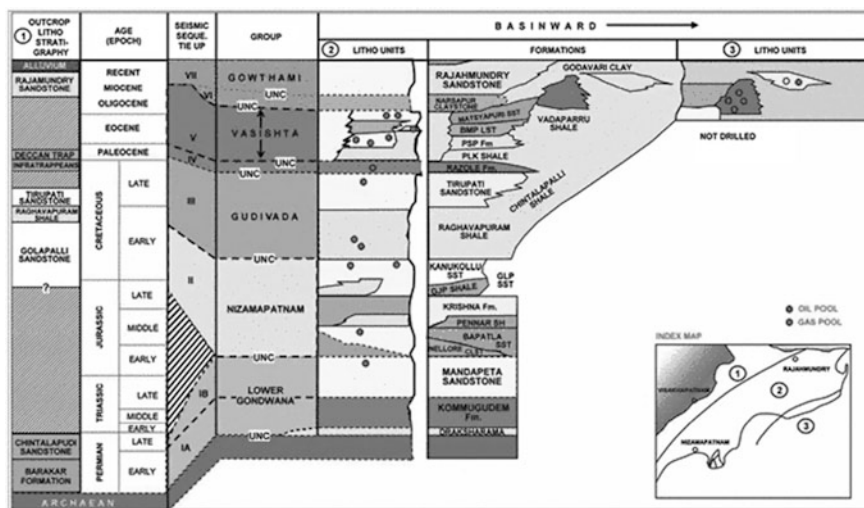


Fig. 2.2 The generalized stratigraphy of Krishna–Godavari basin (after [18, 19]). The Godavari Graben is filled with a maximum of 2.8-km-thick Early Gondwana (Late Permian to Early Triassic) sediments [20]. In between the horst structures, three sub-basins are, namely, Krishna, West Godavari and the East Godavari. The basin is dominated by deltaic plains near the sea–land boundary

Karai Shale Formation ranges in age from Albian to Cenomanian. It consists of a basal limestone unit, which is coralline and reefoidal at some places, overlain by grey to dark grey calcareous, pyritiferous shales with phosphatic nodules. The uppermost part of the formation consists of siltstone and sandstones [1, 4]. The first basin-wide marine transgression took place during Cenomanian and continued up to Maastrichtian. The post-rift thermal subsidence continued throughout remainder of the Cretaceous and Tertiary. This event is represented by extensive marine sedimentation in the rock record of the East Coast basins [6].

The rift-drift (spreading) transition is also marked by the volcanic activity in the Gulf of Mannar, which had started in Cenomanian and continued till Santonian. During early thermal subsidence stage, spanning from Cenomanian to Maastrichtian, these half-grabens were gradually invaded by the sea and were occupied by interconnected seas (Fig. 2.2). *The Paravay Formation*, ranged in age from Turonian to Coniacian, consists of grey to dark grey, hard, compact, massive, fine to medium grained calcareous sandstones. Variegated clays and limestones occur frequently within the sandstone. *Trichinopoly Formation* is confined to Santonian age. It consists of two members, the basal brown, compact, arenaceous shelly limestone with intervening sandstones and grey to brown clays and the upper yellow to brown argillaceous, fossiliferous limestone interbedded with marls and gypseous clays. *The Lakkudi Formation* is of Campanian age. It consists of yellowish to grey and white, fine to medium grained sandstones. *Kallankurichi Formation* is of Early Maastrichtian age. It is made up of limestones ranging from grainstone to wackestone [2, 6, 14]. The lower part is sandy. *Kallamedu Sandstone Formation* belongs to Late Maastrichtian age. The sandstone is yellowish white to white. It grades upwards into ferruginous claystone. The early thermal subsidence stage is marked in the basin by marine transgression. The dark gray shales of *Dhananjayapur Formation* of the Upper Cretaceous age were deposited during this phase. The lithology of the Cretaceous section in the subsurface is predominantly clastic with thin limestone layers over most of the basin. A thick dolomite unit is present over a part of the Pattukottai horst [2, 6, 14]. Eastwards of the horst along the East Coast of India a blanket of Paleocene sediments filled any Cretaceous topography.

In the Middle Eocene, the hard collision of continental India with continental Eurasia took place. In the Early Miocene, continuing shift of India to the North led to rise of the Himalayas to the extent when deposition of sediments of the Ganges began to affect the sedimentation of all the eastern coast of India. *The Niniyur Formation* ranges in age from Paleocene to Early Eocene. It consists of a lower, purple to greyish white sandstone overlain by buff to cream coloured, fossiliferous limestone [2, 14]. Himalayas rose to a great height in the Middle Miocene and sedimentation of the fan of the Ganges dominates deposition processes in offshore zone of the eastern coast. *The Cuddalore Formation* ranges in age from Middle Miocene to Pliocene. It consists of non-marine pebbly sandstone strata in the western part. Towards the coast, this formation becomes more argillaceous with increasing marine influence.

Finally, coastal and deltaic plains of Quarternary age consisting of yellow to grey, fine grained sands and clays are seen over a major part of the land area of the basin between the Precambrian outcrops and the coast line. The shallow marine area of Cauvery coastline is marked by deposition of sands, parallel to the coast, by along shore currents [2, 6, 14]. Mazumdar et al. [21] note that higher smectite contents in sediments of the Krishna-Godavary Basin compared to the Mahanadi Basin suggests a contribution of weathered Decan basalts to sedimentary rocks of the Krishna-Godavari Basin.

2.2 Thermal, Burial and Maturity Histories of the Krishna-Godavari and Mahanadi Basins

2.2.1 Input Data for Modeling

In this chapter we analyze the changes in tectonic, thermal, maturation and generation histories of the basin rocks at transition from the shallow to deep areas of the eastern offshore of India on the example of the Krishna-Godavary and Mahanadi Basins. Consequently, we study burial, thermal, tectonic and maturation histories of the basins on the example of five wells 1, 3, 5, 7, 9 in the shallow offshore (water depth is 10–90 m) and five pseudo-wells located in the deep-water offshore (water depth is 1900–2800 m). Locations of these wells and conjugate pseudo-wells are shown in Fig. 2.3. The first six modeling areas (1–6) are divided from others areas

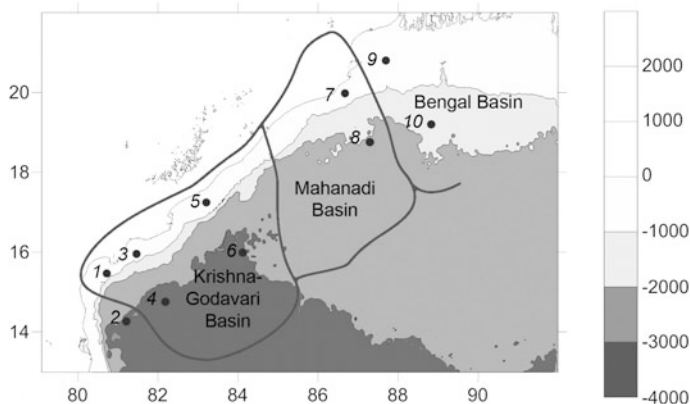
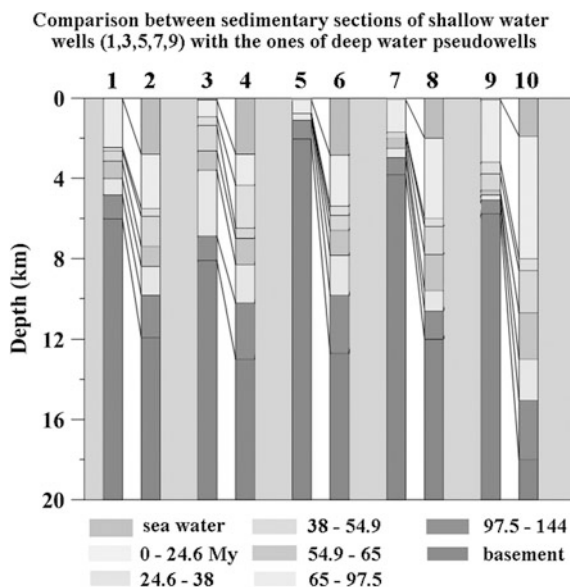


Fig. 2.3 Location of pseudo-wells (1, 3, 5, 7, 9) in shallow offshore near the coast with water depth of 10–90 m and the pseudo-wells (2, 4, 6, 8, 10) in deep offshore (water depth is 1900–2800 m)

Fig. 2.4 Comparison of thickness of sedimentary formations of different age in shallow-sea (wells 1, 3, 5, 7, 9) with the ones in deep sea areas of the north-eastern offshore of India (pseudo-wells 2, 4, 6, 8, 10). (The locations of pseudo-wells are shown in Fig. 2.3.)



(7–10) by the 85° E Ridge [2]. Areas 1 and 2 are in the boundary of the Krishna-Godavary and Palar Basins, and areas 9 and 10 belong to the boundary between the Mahanadi and Bengal Basins (Fig. 2.3; [1]).

A significant part of initial data for modeling consists of description of sedimentary sections of the basins. For the wells: GS-41-1 (1), GS-5-1 (3), KB-4-1B (5), MND-5 (7), NEC-1 (9), these sections were constructed on the base of drilling data for the horizons with reasonable burial depth and seismic data for the deepest horizons of the sections. The sedimentary sections in the deep-water offshore (pseudo-wells 2, 4, 6, 8, 10) are constructed on the base of seismic profiles crossing the areas of these pseudo-wells. Figure 2.4 demonstrates correlations of sedimentary deposits of different age in the areas near coast (wells 1, 3, 5, 7, 9) with the ones in the deep offshore areas (2, 4, 6, 8, 10). Transition from the first group to the second one is accompanied by increase in thickness of sedimentary blanket largely due to contribution of the Miocene-Pliocene section that trends to increase towards the North and the ocean (Fig. 2.4).

The GALO program computes the distribution of temperatures with depth and time from numerical solutions of one-dimensional non-steady heat transfer equations during compaction history of sediments (Sect. 1.1). The domain for temperature calculation has mobile upper boundary that changes during sedimentation or erosion. Petrophysical attributes of the rocks in heat transfer equation change with depth and time (see Sect. 1.1). The GALO system uses a so-called “flat basin approach” which considers variations of temperature only with depth and time and neglects variations in the horizontal (x, y) plane. In spite of this limitation, this approach has some advantages compared to other basin modelling systems because

Table 2.1 Initial model of the continental lithosphere of India (before stretching) used in our modeling as initial model of the margin lithosphere [22–24]

Layer	Granitic			Basaltic	Mantle
Depth of the layer base (km)	1.0	11.0	20	40.0	>40
Density (g/cm^3)	2.75	2.75	2.75	2.90	3.30
Heat conductivity (W/m K)	3.30	3.15	2.80	1.90	$K = f(T)$
Radiogenic heat production (mW/m^3)	3.30	1.40	0.20	0.10	0.00

Remark Dependence heat conductivity K on temperature T in the mantle (function $K = f(T)$) is determined according to Sect. 1.1.2)

it allows you to set the lower boundary of the domain for temperature calculation at great depth (Sect. 1.2).

We simulate heat transfer in the sedimentary section, the underlying lithosphere and asthenosphere down to depths of $ZM = 90\text{--}120$ km. The temperature $TM = 1150\text{--}1170$ °C is maintained at low boundary of the domain (at depth ZM). The principles of computation of the parameters TM and ZM are discussed in Sect. 1.1.4. The model of the lithosphere used in our reconstructions differs from the standard continental lithosphere in Table 1.1 by presence of the thicker granitic layer in the crust. Structure of the lithosphere shown in Table 2.1 is constructed on the base of the data of geological and geophysical studies in the region [22–24].

The gravity-derived crustal models suggests the crust at the eastern Indian shield margin 39–41 km thick, which thins to as much as 20–23 km at the Ocean-Continent Transition in offshore [14]. On the base of this information, the initial crustal thickness of 40 km was taken in our model. It corresponds to the present-day thickness of consolidated crust in undeformed regions of central India. Densities and heat conductivity of the consolidated crust and mantle rocks are presented in Table 2.1 for normal conditions ($P = 1$ atm, $T = 0$ °C). They change with pressure and temperature at numerical simulation of the basin development (Sects. 1.2 and 1.3). Heat conductivity and heat capacity of the mantle rock in our modeling change with temperature according to recent analysis of heat transfer in the mantle (Sect. 1.1.2). The basement described in Table 2.1 was subjected to intense stretching in the Lower and Upper Cretaceous (see below). Radiogenic contribution of the initial consolidated crust is about 23.1 mW/m^2 . It can be significantly less in the modern lithosphere of the passive margin at the areas of the pseudo-wells 2, 4 and 6, where amplitude of the lithosphere stretching could reach 2 and more (Table 2.2).

The temperatures corresponded to paleoclimatic condition (the mean annual temperatures at the sea bottom) are taken at upper boundary of the domain, $Z = 0$. These temperatures are shown in upper parts of Figs. 2.5 and 2.6. They were determined on the base of the paleoclimate data in [25], changes in paleo-latitude of the region under study [2, 6, 14, 26] and variations in the sea depth during the Basin history (curves 4 in Fig. 2.7). Paleoclimate curve of shallow-water offshore areas (wells 1, 3, 5, 7 and 9) reflects just linear increase of the surface mean annual temperature from 15 °C in the Lower Cretaceous to 26 °C at the present time.

Table 2.2 Tectonic and maturation history of the sedimentary basins in the eastern passive margin of India: comparison between shallow and deep shelf

Well number	1 (GS-41-1)	2	3 (GS-5-1)	4	5 (KB-4-1B)	6	7 (MND-5)	8	9 (NEC-1)	10
Zsea (m)	10	2800	90	2800	70	2850	75	2000	80	1900
Zg-h (m)	0	378	0	388	0	366	0	379	0	329
β	1.21	1.92	1.27	2.13	1.04	2.29	1.21	1.61	1.13	2.70
tb (My)	144	144	144	144	286	144	144	144	144	144
zs (m)	6000	9100	8,000	10,200	3800	9850	3700	10,000	5700	16,100
Ro (%)	2.07	2.48	3.88	3.32	1.05	3.49	0.76	2.41	1.13	4.69
Zow (km)	1.89-4.64	2.94-6.61	1.57-4.07	2.60-6.07	1.67-3.80	2.57-5.90	2.35-3.70	3.40-7.45	2.27-5.70	3.10-6.70
tow (My)	15-90	32.6-88	42-70.6	31-74.6	129-286	25-79.6	63.5-144	17.3-64.3	9-144	4.9-38

Remarks Numbers of the wells correspond to Fig. 2.3. tb, zs and Ro are the age, depth and maturity (vitrinite reflectance) of sedimentary rocks at the base of sedimentary cover. Zow and tow the depth and age of the rocks at roof and base of “oil window” ($0.50 \leq Ro \leq 1.30$ %), Zsea modern depth of sea bottom, β is total amplitude of thinning of the consolidated crust. Zg-h depth of lower boundary of zone for the methane gas hydrate stability (its upper boundary is the sea bottom, $z = 0$ m)

Paleoclimatic curve in the deep shelf (pseudo-wells 2, 4, 6, 8, and 10) is determined mainly by change in bottom temperature related to the variations in the sea depth (Figs. 2.5 and 2.6).

The distribution of the basement and sediment rock densities with depth is calculated at each time step of the Basin development over entire depth interval of computation. In addition, variations in tectonic subsidence of the Basin are computed during its burial history by two methods (Sects. 1.2 and 1.3; Fig. 2.7). In the first (solid line 2 in Fig. 2.7), tectonic subsidence is calculated by removing sediment and water load on the basement surface according to Eq. (1.11). In the second method (dashed line 3 in Fig. 2.7) changes in amplitude of the tectonic subsidence relative to its initial value are computed by considering the time-dependent variations in density distribution of the basement rocks (Eq. (1.13)). If isostatical response of the lithosphere on external and internal load is assumed, both tectonic variations presented by the curves 2 and 3 in Fig. 2.7 must coincide. We fit the amplitude and duration of thermal activation and stretching of the lithosphere to ensure this coincidence (Sect. 1.3). Therefore, the GALO program allows an analysis of the thermal evolution of the basins which had been undergone by repeated phases of the lithosphere heating and extension, and is not limited to simple models of the lithosphere cooling (see Sect. 1.3).

2.2.2 Thermal and Maturation Histories of Sedimentary Basins in the Eastern Shelf of India: Results of Modeling

The reconstructed thermal history of the margin lithosphere is demonstrated in Fig. 2.8 on the example of the well 1 (well GS-41-1) and pseudo-well 2 presented shallow and deep shelf of the Krishna-Godavari Basin correspondingly (Fig. 2.3). Figure 2.8a, c show variations in heat flow through the surfaces of sedimentary blanket (solid line) and the basement (dashed line). In our reconstructions, heat flow at the Basin initiation was about 120 mW/m^2 . It is close to mean heat flow in axial zones of continental rifting. The history of the Basin tectonic subsidence differs considerably in the deep and shallow-water offshore areas (Figs. 2.7 and 2.8). According to our analysis, an amplitude of lithosphere extension, β , is 1.21 in the area of the well 1 (GS-41-1) with sea depth of about 10 m, whereas β reaches 1.92 in the pseudo-well 2 with sea depth of about 2800 m (Fig. 2.7; Table 2.2). In the lithosphere of the deep shelf, the crustal thickness reduces from an initial value of 40 to 29 km at present time. The later includes 9.1 km of the modern sedimentary cover (see “MOHO” line in Fig. 2.7b). This reduction in thickness of the consolidated crust ensured the deepening of the sea up to 2.8 km in the Cretaceous. At the same time, the crust in the shallow-water offshore reduces only to 38 km with thickness of sedimentary blanket 6 km (left Fig. 2.7b). High amplitude of lithosphere stretching in the deep shelf corresponds to great sea depth (Table 2.2).

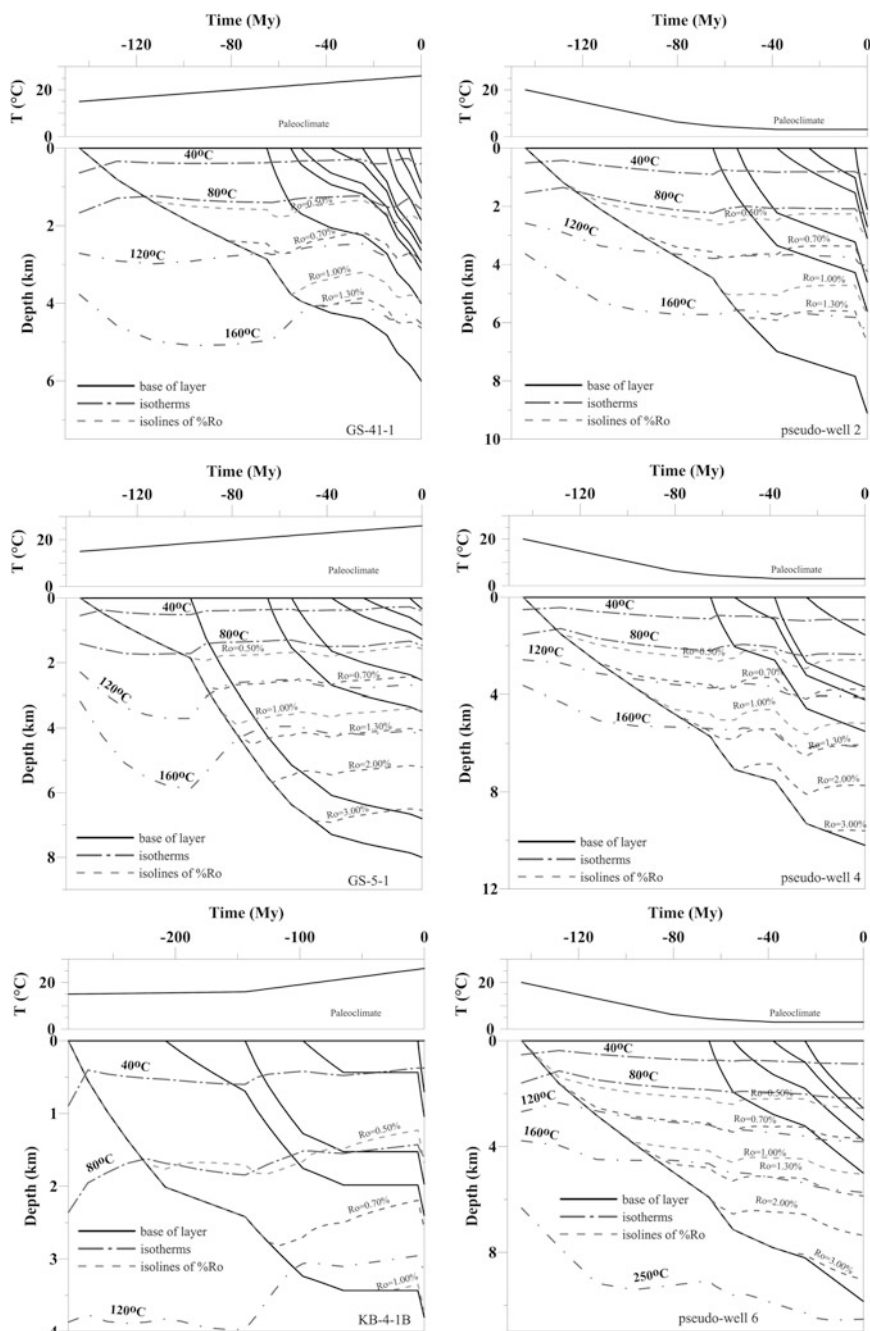


Fig. 2.5 Variations in mean-annual surface temperature (mean-annual temperature at sea bottom) (*upper figures*) and burial, thermal and maturation histories (*lower figures*) of sedimentary sections in the Krishna-Godavari Basin (wells 1, 3, 5, pseudo-well 2, 4, 6; Fig. 2.3)

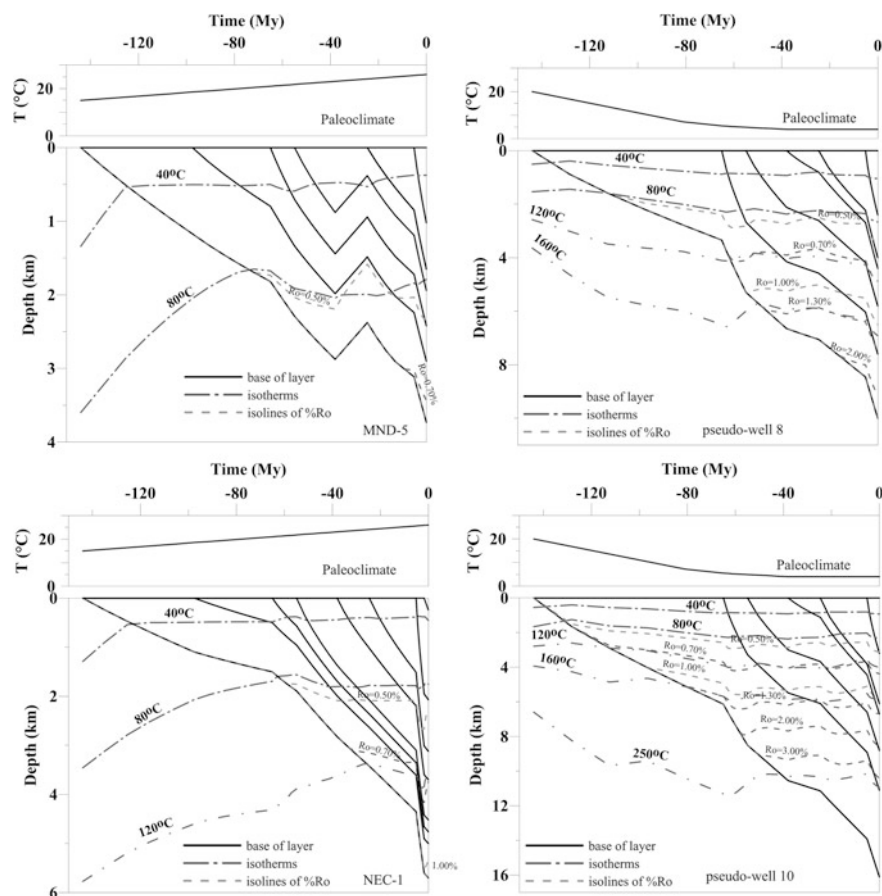


Fig. 2.6 Variations in mean-annual surface temperature (mean-annual temperature at sea bottom) (*upper figures*) and burial, thermal and maturation histories (*lower figures*) of sedimentary sections in the Mahanadi Basin (wells 7, 9, pseudo-well 8, 10; Fig. 2.3)

But highest amplitude of extension $\beta = 2.7$ is reached in pseudo-well 10 in north-western part of the Bay of Bengal with sea depth of 1900 m. Such amplitude corresponds to depth of the Mochorovich boundary about 31 km and is related partly to anomalous thickness of sedimentary section (more than 16 km).

The calculated temperature distribution in present-day sedimentary section of the area 1 (GS-41-1) is shown in Fig. 2.9. by solid line. Two temperatures measured in the GS-41-1 well are shown by stars. The GS-5-1 and GS-41-1 wells are located in a relatively narrow area (may be local fracture) of the south-eastern coast of India with a high modern heat flow [27, 28]. They are characterized by higher temperatures at the same depth compared with pseudo-wells 2 and 4.

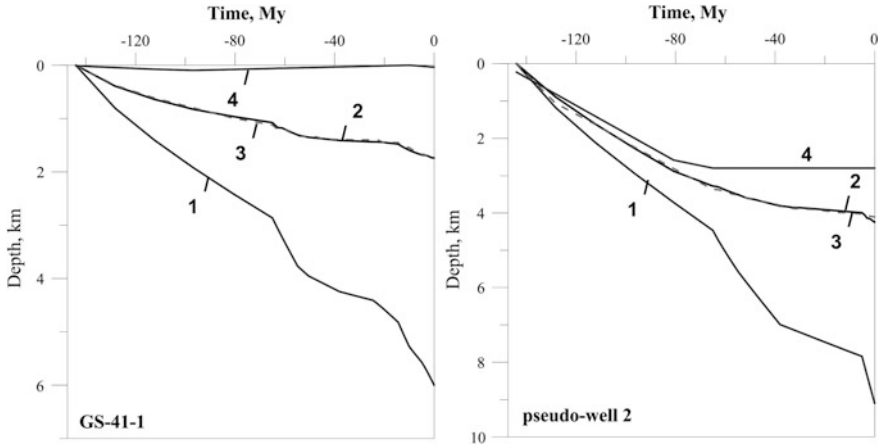


Fig. 2.7 Tectonic subsidence of the basement surface in the areas of the well 1 (well GS-41-1) and pseudowell 2 located in the shallow and deep shelf of the Krishna-Godavari Basin (Fig. 2.3) and calculated in the local isostasy approach. 1 depth of the base of sedimentary cover (or the depth of the basement surface) computed by usual “backstripping” procedure; 2 (*upper solid line*)—tectonic subsidence of the basin calculated by removing the sediment and water load from the basement surface (Eq. (1.11)); 3 (*upper dashed line*)—tectonic subsidence calculated by consideration of time-variations in density profile in the basement (Eq. (1.13)); 4 sea depth

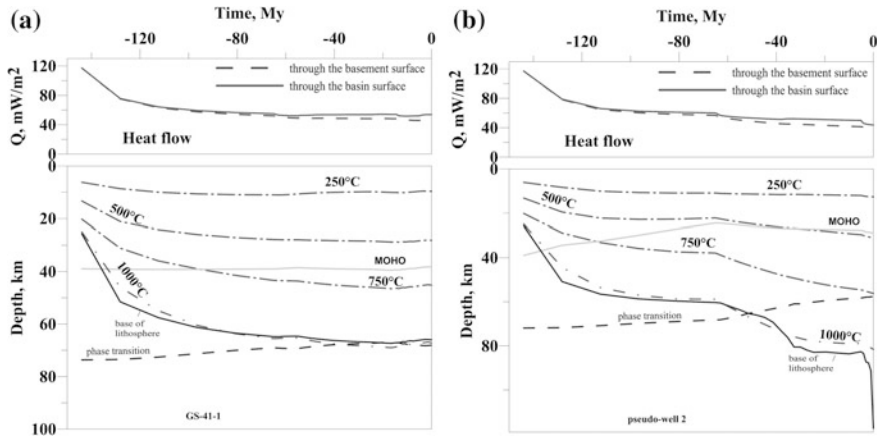


Fig. 2.8 Variations in heat flow (a) and thermal state of the lithosphere (b) reconstructed numerically in the GALO system for the well 1 (well GS-41-1) and pseudowell 2 located in shallow and deep shelf of the Krishna-Godavari Basins (Fig. 2.3). **a** The heat flows through the sediment and basement surfaces; difference between the flows is mainly due to radiogenic heat generation in sediments. **b** Long dashed lines are isotherms. The “moho”-line is the base of the crust. The “phase transition” line is the location of “spinel peridotite—garnet peridotite” compositional transition in the mantle (Eq. (1.16)). *Base of the lithosphere*—depth of intersection of the current geotherm of the lithosphere with the solidus of peridotite with 0.2 % H_2O (Eq. (1.4))

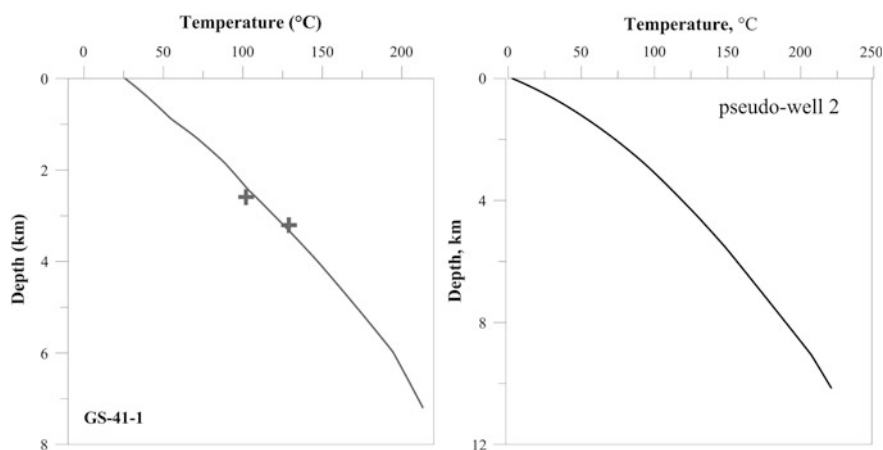


Fig. 2.9 Calculated (solid lines) and measured (crosses) temperatures with depth in the modern sedimentary sections of the well 1 (well GS-41-1) and pseudowell 2 located in the shallow and deep shelf of the Krishna-Godavari Basin (Fig. 2.3)

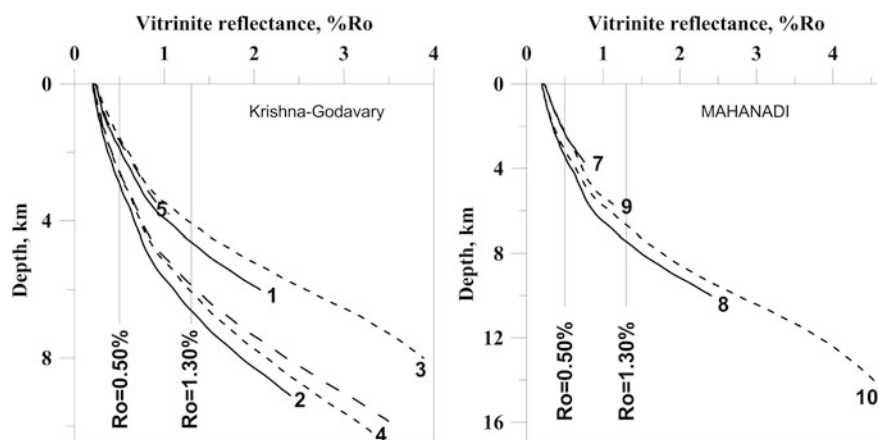


Fig. 2.10 Calculated variations in vitrinite reflectance with depth in modern sedimentary sections of Krishna-Godavari Basin (wells 1, 3, 5, pseudo-wells 2, 4, 6; *left figure*) and Mahanadi Basin (wells 7, 9, pseudo-wells 8, 10; *right figure*). Numbers correspond to numbers of wells and pseudo-wells in Fig. 2.3. The oil window ($0.50 \leq Ro \leq 1.30\%$) is shown by vertical lines

Main results of the modeling in different areas of the Krishna-Godavari and Mahanadi Basins are presented in Figs. 2.5, 2.6 and 2.10, Table 2.2. They give an opportunity to compare changes in temperature regime of sedimentary sections and degree of maturation of organic matter in sedimentary rocks at the transition from shallow to deep-water offshore.

Our modeling suggests that sedimentary rocks in the shallow shelf are hotter than the rocks at the same depth in the deep shelf. However, the

situation is reversed for rocks of the same age. These rocks in deep-water offshore are characterized by greater depth, temperatures and maturity level, than the rocks of the same age in the shallow shelf. This trend is obvious for areas 5–10 but it is less obvious for areas 1–4 because the wells 1 and 3 are located in a local region of elevated heat flow [27, 28]. The modeling shows that intensive sedimentation from the Gang River in the Miocene-Pliocene led to considerable subsiding of “oil window” in both basins (Table 2.2), but its influence is more pronounced in the Mahanadi basin, especially in the pseudo-well 10 (Figs. 2.5, 2.6 and 2.10, Table 2.2). Top of the “oil window” ($R_o = 0.50\%$) in present section is deeper in the deep offshore than in the shallow one by nearly 1 km, whereas base of the “window” ($R_o = 1.30\%$) is deeper by 1–3.5 km in comparison with the shallow shelf. As a whole, the rocks located within the “oil window” are younger in the deep shelf areas (Figs. 2.5, 2.6 and 2.10; Table 2.2). Summing up the results of the section, we note that the deepening of the “oil window” with distance from the coast, and with approach to the mouth of the Ganges River is mainly due to increase of the Miocene sedimentation rates (Figs. 2.4, 2.5 and 2.6).

2.3 A Comparison Temperature and Maturation Histories of the Probable Source Rocks in the Basins in the Shallow and Deep-Sea Areas

This section gives a short comparison between temperature and maturation conditions in the probable source rocks of the shallow- and deep-sea areas in the Krishna- and Mahanady-Basins. It is often found in the literature an assessment of maturation degree of organic matter not only by computation or measurement of vitrinite reflectance, but also by estimation of the transformation degree in clay minerals (smectite to illite transition). We used the results of our simulation to compare both methods of maturity estimation.

2.3.1 *Estimation of Smectite/Illite Ratio During Diagenesis of Clays*

Evaluation a degree of transformation smectite to illite computing a ratio smectite/illite is often used together with calculation of vitrinite reflectance to estimate organic matter maturity. Smectite to illite transition is the most important mineral reactions during diagenesis of clay. Usually, smectite is found in fine-grained sediments at shallow depths. During diagenesis and deeping, smectite generally turns into illite, releasing silicon, water and cations. Earlier one-step

models of the smectite to illite transformation [29–31] did not demonstrate a good agreement with observations at application to geological time scale. The two-step model of smectite transformation proposed in the papers [32–34] describes geological situation considerably better than the previous one-step models. We use the two-step model of Velde and Vasseur [32–34] to compute a change of fraction of smectite in mixture smectite/illite during burial history of the probable source formations. Our results give an opportunity to compare the values of vitrinite reflectance, Ro%, with corresponding ratios Smectite/Illite and estimate a possibility to use this relationship in basin analysis. In the model of [33], take a place two reactions: $X \rightarrow Y$ (the first reaction) and $Y \rightarrow Z$ (the second reaction). At the first reaction, smectite layer belong to X becomes illite. Therefore X disappears but the new illite joints with neighbouring smectite forming new sub-row Y consisted of one smectite + one illite. This reaction is clear to correspond to transformation of initial mineral ($R = 0$) with non-ordering smectite to ordering mineral ($S = 1$). If only the first reaction ($X \rightarrow Y$) would be active, it could lead to the mineral $R = 1$ with 50 % smectite. But there is the second reaction ($Y \rightarrow Z$) when smectite layer belong to Y becomes illite and forms sub-layer Z (two illites). This reaction describes the process of gradual illitization of mineral $R = 1$ and it competes with the first reaction. Then, the equations ruled the reactions can be described as:

$$dX/dt = -k_1 \cdot X; \quad \text{where } k_1 = A_1 \cdot \exp(-E_1/RT(t))$$

$$dY/dt = k_1 \cdot X - k_2 \cdot Y, \quad \text{where } k_2 = A_2 \cdot \exp(-E_2/RT(t))$$

Then, total content of smectite in rock is:

$$S(t) = X(t) + (Y(t)/2)$$

Initial values $X = X_0$, $Y = Z = 0$.

Solution of the above equations is:

$$X(t) = X_0 \cdot \exp\left[-\int_0^t k_1(t') \cdot dt'\right]$$

$$Y(t) = X_0 \cdot \exp\left[-\int_0^t k_2(t') \cdot dt'\right] \times \int_0^t k_1(t') \cdot \exp\left(\int_0^{t'} [k_2(t'') - k_1(t'')] \cdot dt''\right) \cdot dt'$$

Parameters of two reactions (A_1 , E_1 , A_2 , E_2) are determined from comparison of geological data with the values S calculated in the model. According to [34] they are:

$$\ln(A_1) = 24.4 \pm 0.6 \cdot \ln(\text{Ma}^{-1}); \quad E_1 = 76.8 \pm 1.7 \text{ kJ/mole}$$

$$\ln(A_2) = 3.6 \pm 0.6 \cdot \ln(\text{Ma}^{-1}); \quad E_2 = 22.2 \pm 2.0 \text{ kJ/mole}$$

The two-step model with the above parameters was used in our computations. It describes the observed geological data (S) better than the previous one-step model.

2.3.2 Comparison of Thermal and Maturation Histories of the Probable Source Rocks

Figure 2.11 demonstrates a comparison in temperature histories of the main probable source rocks in the shallow (w. GS-41-1) and deep (pseudo-well 2) shelf of the Krishna-Godavary Basin.

Figures 2.12 and 2.13 demonstrates similar comparison for maturity degree of organic matter and transformation degree in clay minerals. The comparison shows that the probable source rocks of Cretaceous and Eocene are buried at greater depth and characterized by more high temperatures in the deep-sea areas than in the shallow-sea ones.

The comparison shows that the probable source rocks of Cretaceous and Eocene located at great depth in the deep shelf are characterized by more high maturity level and clay transformation ratios than in the shallow shelf.

Figures 2.14, 2.15 and 2.16 demonstrate similar comparison for two areas of the Mahanadi Basin. The great difference in the burial histories of the NEC-1 and pseudo-well 10 areas (Fig. 2.6) results in considerable difference of these areas in thermal and maturity histories of the formations.

The probable source rocks of Cretaceous and Eocene are burried at greater depth and characterized by more high temperatures in the deep-sea areas in the Mahanadi Basin than the rocks in the shallow-sea areas of the Basin. This effect is especially considerable close to the Gange mouth.

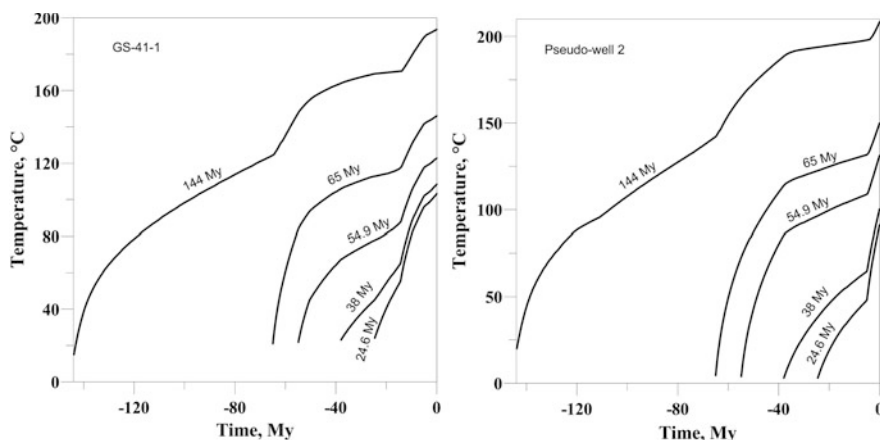


Fig. 2.11 Comparison between temperature histories of probable source rocks in the shallow (w. GS-41-1) and deep (pseudo-well 2) sections of the Krishna-Godavary Basin

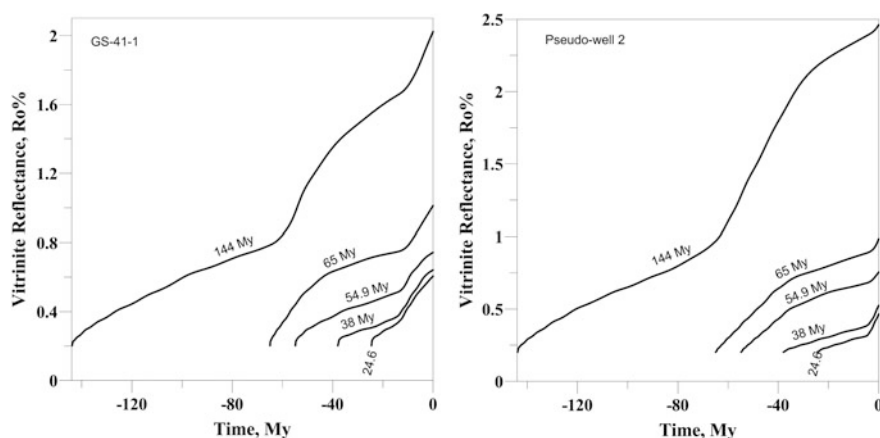


Fig. 2.12 Comparison of catagenesis history of probable source rocks in the Krishna-Godavary Basin in the shallow (GS-41-1) and deep (pseudo-well 2) areas

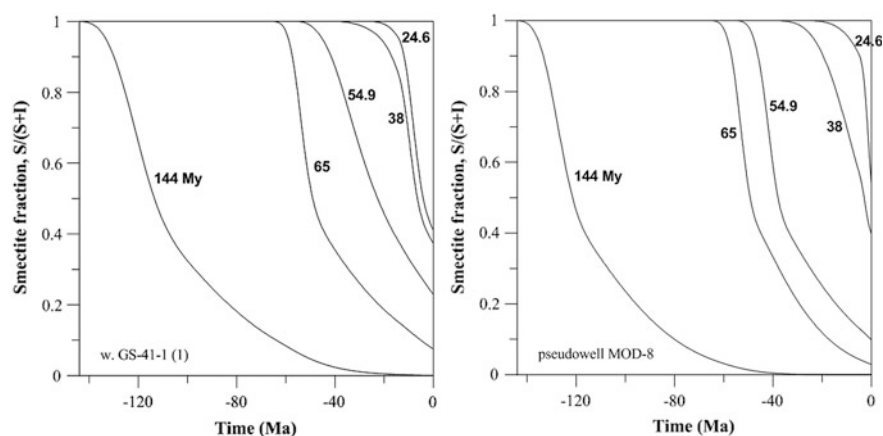


Fig. 2.13 Comparison between smectite content in the burial history of the probable source rocks in the Krishna-Godavary Basin in the shallow (GS-41-1) and deep (pseudo-well 2) areas

2.3.3 *Correlation Between Smectite/Illite Transformation and Ro%*

It would be interesting even for the basins of the Eastern shelf of India to establish whether there is a definite correlation between vitrinite reflectance %Ro and the ratio $S/(S + I)$ in clays. Correlation between Smectite/Illite ratio and rock temperatures can be seen from comparison of results in Figs. 2.11 and 2.14 with Figs. 2.13 and 2.16. Hunner [35], analyzing the process in the Mexico Bay says that the start of the smectite to illite transformation corresponds to the temperatures from 58 to 92 °C.

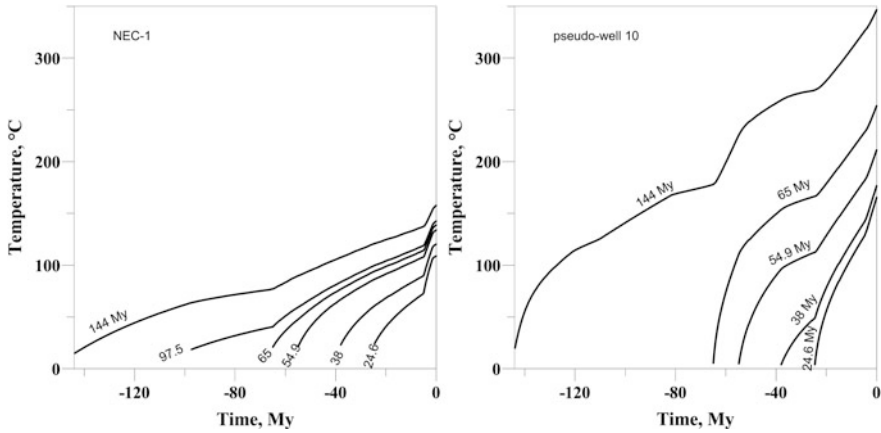


Fig. 2.14 Comparison of temperature histories of probable source rocks in the Machanady Basin in the NEC-1 and pseudo-well 10 areas

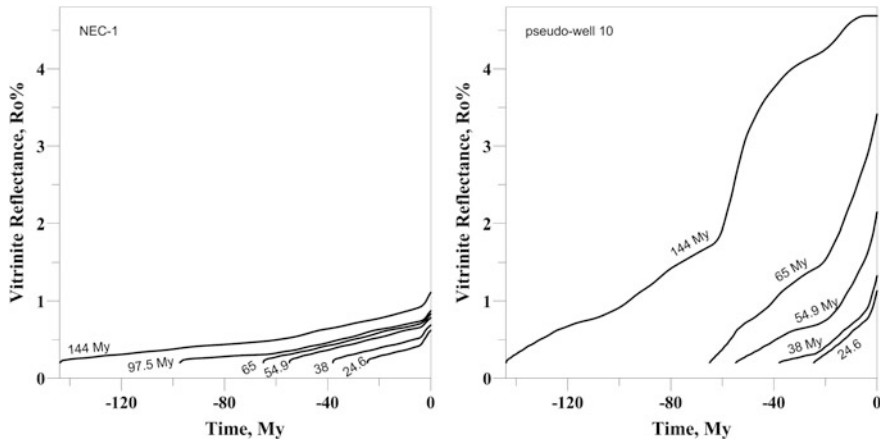


Fig. 2.15 Comparison of catagenesis histories of probable source rocks in the Machanady Basin in the NEC-1 and pseudo-well 10 areas

Our calculations suggests temperatures from 50 to 70 °C. For finish of the transformation Hunner [35] suggests wide temperature interval: from 88 to 142 °C. He says that smectite loses last water layer at the temperatures from 172 to 192 °C. The latter is in a rather good agreement with our calculations in the two-step model of clay transformation. But it is necessary to keep in mind that the process of transformation of smectite to illite is kinetic and must be ruled not only by temperature but the time too. By this reason, the correlation of smectite/illite transformation with temperature must be very approximate. It is more interesting to consider the correlation of the smectite/illite ratio with vitrinite reflectance Ro% because both

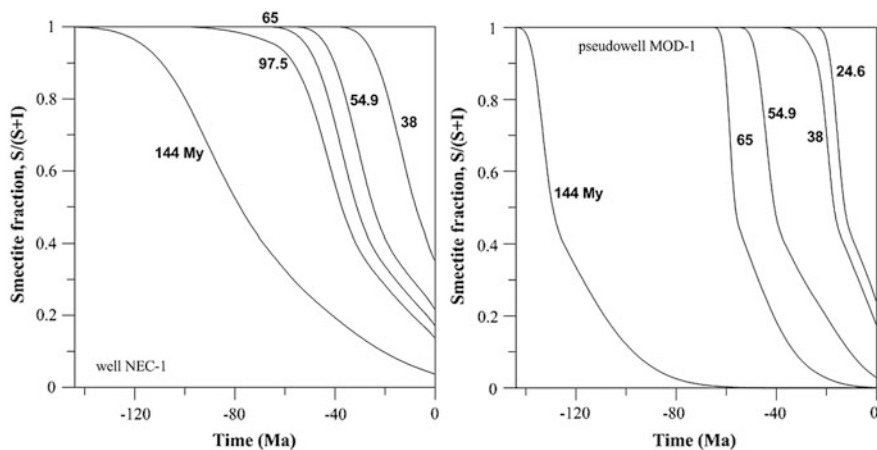


Fig. 2.16 Comparison between smectite content in the burial history of the probable source rocks in the Machanady Basin in the NEC-1 and pseudo-well 10 areas

processes of smectite transformation and vitrinite maturation are the kinetic processes. Figure 2.17 presents the fraction of smectite in Smectite/Illite mixture calculated in two-step model of smectite transformation as a function of vitrinite reflectance for different sedimentary formations of the GS-41-1 well (left Fig. 2.17) and for the Low Cretaceous formations of southernmost and northernmost areas under study (wells GS-41-1, Nec-1, and pseudo-wells 2 and 10 (right Fig. 2.17).

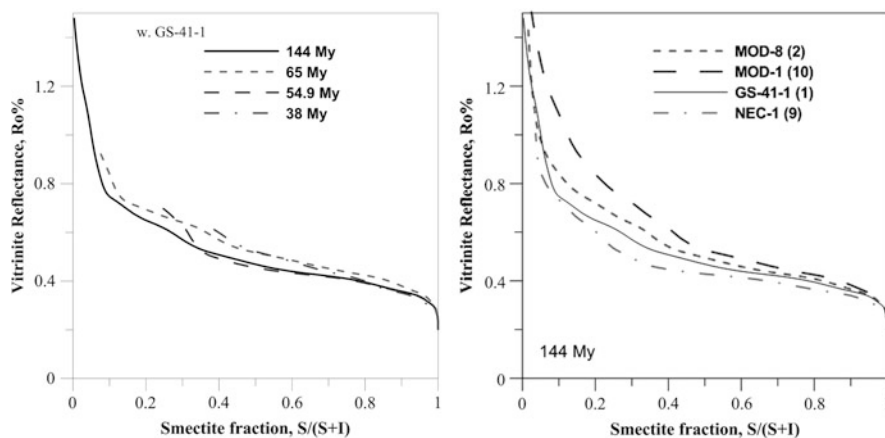


Fig. 2.17 The fraction of smectite in Smectite/Illite mixture calculated in two-step model of smectite transformation as a function of vitrinite reflectance for different sedimentary formations of the GS-41-1 well (*left figure*) and for the Low Cretaceous formations in the southernmost and northernmost areas under study (wells GS-41-1, Nec-1, pseudo-wells 2 and 10; *right figure*)

Figure 2.17 shows that at quality agreement of the curves in the left Fig. 2.17 there is considerable scattering in Ro% data at fixed ratio $S/(S + I)$ for burial histories in different areas of the Basins (right Fig. 2.17). Figure 2.17 demonstrates that different kinetics of vitrinite maturation and Smectite/Illite transformation do not suggest a single universal relationship between Ro% and the $S/(S + I)$ ratio.

2.4 Hydrocarbon Generation by Probable Source Rocks in Shelf Areas of the Krishna-Godavary and Mahanady Basins

Large prospects of oil and gas generation follow from the study of the source rocks in the East coast of India [8, 18, 36]. Geochemical study shows that the Cretaceous source rocks of the margin are characterized by TOC = 0.75–3.00 % and contain predominantly kerogen of type III with initial potential 100–300 mg HC/g TOC [26, 36, 37]. The Early Cretaceous shales of the Pennar formation are believed to be source rocks for the overlying Krishna formation. As mentioned above, shales of the Middle Cretaceous Raghavapuram formation mark the first marine transgression and start of spreading. The shales of the Middle and Upper Cretaceous contain predominantly organic matter of type III with little admixture (30 %) of type II with TOC about 1.5 % [18, 36]. They are considered as good source rocks. It is believed that initial potential of these source rocks was HI = 225 mg HC/g TOC. In particular, the Late Cretaceous shales of the Chintalapalli formation are believed to be source rocks for hydrocarbon accumulations in the Tirupati sandstones [8, 18]. Paleocene shales in the Krishna-Godavari Basin contain kerogen of type III with modern TOC \approx 1.4 % whereas the same rocks in the Mahanadi Basin contain an organic matter of type III mixed with type II with TOC approximately 2 % [12]. The Eocene/Oligocene shales of the Vadaparru formation are considered as source rocks for hydrocarbon accumulations in the Ravva formation of the Miocene-Pliocene age. The Eocene shales in both basins are characterized by kerogen of type III with TOC = 1.5 % in the Krishna-Godavari Basin and 2 % in the Mahanady Basin. The Oligocene shales contain kerogen of type III with TOC = 2 % in the Mahanady Basin and the same kerogen mixed with type II with TOC = 2.5 % in the Krishna-Godavari Basin. Kerogen of type III with TOC = 1.3–1.5 % is typical for Miocene shales in both basins [12, 26, 37, 38].

As mentioned above, the content of organic matter in present-day sedimentary section of the Eastern margin of India can range widely: from 0.3 to 6 % [8, 18, 36]. TOC = 1.5 % was accepted in our assessments as reasonable mean value of the TOC (Tables 2.3 and 2.4). The calculated values of TOC at initiation of burial history of the formations are shown in Tables 2.3 and 2.4 in the TOCinit column. Difference between TOCinit and TOC depends on type of kerogen, its initial hydrocarbon potential and realization degree of this potential (maturity level of organic matter) [39–41]. In accordance with the above information, we suggest that

Table 2.3 Maturity level and realization history of hydrocarbon potential in sedimentary sections 1–6 in the Krishna-Godavary Basin (results of modelling)

t	Z	T	Ro	Hi	Ht	Hho	Hlo	Hoil	Hgas	TOC	TOCinit	t _{0.5}	t _{1.30}
My	m	°C	%	mg HC/g TOC									
Pseudo-well 1 (well GS-41-1) sea depth 10 m													
144	6000	194	2.04	160	134	7.6×10 ⁻⁴	1.02	1.02	80.6	1.5	1.73	113	42
65	4000	146	1.02	225	130	33.9	42.1	76	27.8	1.5	1.72	52	—
54.9	3140	123	0.72	225	34.9	27.3	41.2	31.5	3.2	1.5	1.55	17	—
38	2630	109	0.64	160	3.14	2.59	0.177	2.77	0.365	1.5	1.50	8.5	—
24.6	2450	103	0.61	225	5.49	4.07	0.896	4.97	0.524	1.5	1.51	6.5	—
Pseudo-well 2 sea depth 2800 m													
144	9100	207	2.37	160	144	6.7 × 10 ⁻⁵	0.021	0.021	91	1.5	1.75	120	51
65	5600	149	0.96	225	114	46.8	30.1	76.9	20.4	1.5	1.69	48	—
54.9	4600	130	0.75	225	36.3	28.4	4.27	32.7	3.34	1.5	1.56	34	—
38	3100	99.5	0.52	160	0.533	0.463	0.0092	0.473	0.06	1.5	1.50	0.55	—
Pseudo-well 3 (well GS-5-1) sea depth 90 m													
144	8000	249	3.85	160	160	0	0	0	106	1.5	1.79	97	74
97.5	6800	224	3.15	225	223	0	0	0	135	1.5	1.90	87	64
65	3500	139	1.00	225	124	36.4	38.6	75	25.6	1.5	1.71	53	—
54.9	2540	111	0.70	225	21.7	17	2.69	19.7	1.96	1.5	1.52	35	—
38	1270	73	0.43	160	0.0269	0.0235	2.4 × 10 ⁻⁴	0.0239	0.003	1.5	1.50	—	—
Pseudo-well 4 sea depth 2800 m													
144	10,200	230	3.28	160	158	0	0	0	104	1.5	1.78	—	—
65	5500	147	1.10	225	145	10.9	58.1	69.1	37.8	1.5	1.76	—	—
54.9	4200	129	0.75	225	37.6	29.3	4.45	33.8	3.48	1.5	1.56	—	—
38	3700	110	0.68	160	4.72	3.8	0.35	4.15	0.559	1.5	1.51	—	—
24.6	1550	58	0.35	225	0.00314	0.00184	0.00105	0.00289	0.00026	1.5	1.50	—	—
(continued)													

(continued)

Table 2.3 (continued)

t	Z	T	Ro	Hi	Ht	Hho	Hlo	Hoil	Hgas	TOC	TOCinit	t _{0,5}	t _{1,30}
Pseudo-well 5 (well KB-4-1B) sea depth 70 m													
286	3800	134	1.03	160	51.1	10.5	17.2	27.7	12.7	1.5	1.58	223	–
208	2400	101	0.66	160	3.59	2.94	0.226	3.17	0.421	1.5	1.51	100.5	–
144	1970	91	0.57	160	1.21	1.05	0.0245	1.075	0.136	1.5	1.50	68.5	–
Pseudo-well 6 sea depth 2850 m													
144	9850	240	3.45	160	159	0	0	0	105	1.5	1.78	133	86
65	5000	144	0.97	225	116	45.3	31.3	76.6	21.2	1.5	1.70	49	–
54.9	3750	118	0.71	225	22.7	17.8	2.79	20.6	2.05	1.5	1.52	17	–
38	3000	100	0.57	160	1.41	1.22	0.0343	1.25	0.16	1.5	1.50	5.7	–
24.6	2550	90	0.50	225	0.745	0.494	0.184	0.678	0.068	1.5	1.50	–	–

Remarks *t* age of the formation in My. *z* depth in m. *T* calculated temperature in °C. *Ro* calculated value of vitrinite reflectance in % (*z*, *T*, *Ro*-values belong to the present-day section of the basin, *t* = 0 in Figs. 2.5 and 2.6). *Hi* initial potential of HC generation by the rocks of the formation; *Ht* total realization of the potential, *Hho*, *Hlo* and *Hoil* generation of heavy and light oil and total oil correspondingly; *Hg* gas generation (in mg HC/g TOC). The values of *Ht*, *Hho*, *Hlo*, *Hoil* and *Hgas* present total generation of corresponding hydrocarbons to present time computed under condition that generated hydrocarbons have not leaved the porous space of the source rocks. *t*₁, *t*₂ times of enter and leaving the “oil windows” (0.50 % ≤ *Ro* ≤ 1.30 %) by the rock. In the Tables 2.3 and 2.4, initial potential *HI* = 225 mg HC/g TOC corresponds to the mixture of 30 % standard marine kerogen of type II with initial hydrocarbon potential 377 mg HC/g TOC and 70 % standard kerogen of type III with initial hydrocarbon potential 160 mg HC/g TOC; *HI* = 160 mg HC/g TOC corresponds to the standard kerogen of type III with initial hydrocarbon potential 160 mg HC/g TOC. The kinetic spectra for HC generation by standard kerogen of types II and III in the frame of 4-th fraction system (heavy and light oil, gas and coke) were used in computations of HC generation (see text)

Table 2.4 Maturity level and realization history of hydrocarbon potential in sedimentary section 7–10 in the Mahanady Basin (results of modelling)

t	Z	T	Ro	Hi	Ht	Hho	Hlo	Hoil	Hgas	TOC	TOCinit	t _{0.5}	t _{1.30}
My	m	°C	%	mg HC/g TOC						mg OM/g rock		My ago	
Pseudo-well 7 (well MND-5) sea depth 75 m													
144	3730	125	0.75	160	10.4	7.92	1.11	9.03	1.31	1.5	1.52	70.5	–
97.5	2900	103	0.59	225	4.3	3.15	0.737	3.89	0.414	1.5	1.51	11.5	–
65	2420	92	0.51	225	0.975	0.659	0.226	0.885	0.090	1.5	1.50	0.5	–
54.9	1940	83	0.44	225	0.197	0.122	0.0582	0.181	0.017	1.5	1.50	–	–
Pseudo-well 8 sea depth 2000 m													
144	10,000	211	2.37	160	145	6.6×10^{-5}	0.0206	0.0206	91.4	1.5	1.75	107	46
65	7600	179	1.34	225	175	0.284	71	71.3	53.2	1.5	1.82	54	0.6
54.9	5800	139	0.82	225	64.5	47.5	8.45	55.9	6.67	1.5	1.60	27	–
38	4400	115	0.64	160	3.08	2.55	0.171	2.72	0.357	1.5	1.50	4.4	–
24.6	4000	107	0.58	225	3.90	2.85	0.671	3.52	0.375	1.5	1.51	2.0	–
Pseudo-well 9 (well NEC-1) sea depth 80 m													
144	5700	158	1.12	160	66.2	6.19	25.5	31.7	18.4	1.5	1.61	59.5	–
97.5	5000	143	0.88	225	85.2	54.4	14.4	68.8	10.7	1.5	1.64	35.5	–
65	4760	139	0.83	225	70.9	50.6	9.88	60.5	7.7	1.5	1.61	30.5	–
54.9	4520	134	0.79	225	52.7	40.3	6.38	46.7	5.11	1.5	1.58	24	–
38	3700	121	0.69	160	5.81	4.63	0.477	5.1	0.694	1.5	1.51	7	–
Pseudo-well 10 sea depth 1900 m													
144	16,100	342	4.69	160	160	0	0	0	106	1.5	1.79	138	80.7
65	11,100	251	3.32	225	224	0	0	0	136	1.5	1.93	56.5	27
54.9	8800	209	2.08	225	206	5.7×10^{-4}	0.863	0.864	118	1.5	1.89	39	7.7
38	6700	175	1.29	160	94.1	0.678	38.4	39.1	29.8	1.5	1.66	16.5	–
24.6	6100	164	1.10	225	148	14.1	57.9	72.0	37.9	1.5	1.76	12.6	–

See remarks to Table 2.3

kerogen of type III with $HI = 160$ mg HC/g TOC was typical for Lower Cretaceous (144 My) and Upper Eocene (38 My) rocks, whereas mixture of 30 % kerogen of type II ($HI = 377$ mg HC/g TOC) with 70 % kerogen of type III ($HI = 160$ mg HC/g TOC) characterizes organic matter of the Middle and Upper Cretaceous (65 My), Upper Paleocene (54.9 My) and Upper Oligocene (24.9 My) rocks in Tables 2.3 and 2.4 and Figs. 2.11, 2.12, 2.13 and 2.14. Algorithms for computing the yields of different hydrocarbon fractions are discussed in detail in [42, 43] and Chap. 3.

Tables 2.3 and 2.4 show the capacity of the main source rocks in the Eastern continental margin of India to generate heavy and light oil and gas estimated in the GALO system of basin modeling. In addition to age, the depth, temperature and maturation level of the rocks, computed for present-day section of the basin, are in these Tables. H_t , H_{ho} , H_{lo} , H_{oil} , and H_{gas} in Tables 2.3 and 2.4 are total generation of hydrocarbons, heavy and light oil, oil and gas to present time, computed in the frame of the 4-fractional model of kerogen cracking (light and heavy oil, gas and coke). We used the kinetic spectra for cracking of kerogen of types II and III in the 4-fractional model, that was developed in the French Oil Institute (Paris) and are applied in a widespread modeling package MATOIL. Note again that Tables 2.3 and 2.4 present the total generation of hydrocarbons of different types reached to current time. Parameters $t_{0.5}$ and $t_{1.30}$ in the tables are the calculated times of entering in “oil window” ($R_o = 0.50$ %) and leaving it ($R_o = 1.30$ %). Now we consider shortly the generation properties of the source rocks beginning with the Cretaceous.

Variations in maturity level of organic matter during burial history of the rocks at the base of the Cretaceous proposed by modeling for different areas of the East margin are shown in Figs. 2.5 and 2.6. These figures and Tables 2.3 and 2.4 allow comparison of maturity levels of rocks in the shallow- and deep-water offshore. The modeling shows that organic matter in the Lower Cretaceous rocks reached rather high maturity level ($R_o > 2.3$ %) in all considered areas of the deep-water offshore (pseudo-wells 2, 4, 6, 8, 10). Such maturity level corresponds to total destruction of heavy and light oil as result of secondary cracking (Fig. 2.11; Tables 2.3 and 2.4). Destruction of oil occurred in deep offshore not later than the Oligocene (Fig. 2.18). Close situation is for the pseudo-wells 1 (w. GS-41) and 3 (w. GS-5-1) located in the shallow offshore within the deep aulocagen in the region with the non-typical high modern heat flow (Fig. 2.18; Table 2.3). Here, the Low Cretaceous rocks are gas prone (Table 2.3). But in others pseudo-wells of shallow offshore (5, 7, 9), these rocks are characterized by a considerable lower maturity level of organic matter (especially in the KB-4-1B well, located on local horst) and could be oil prone (Fig. 2.18; Tables 2.3 and 2.4).

Figure 2.19 presents a history of realization of hydrocarbon potential of the Upper Cretaceous source rocks on the example of the same pairs of pseudo-wells: 1, 2 and 9, 10. Tables 2.3 and 2.4 and Fig. 2.19 show that the Upper Cretaceous rocks are oil prone. They are actively generating oil. The exception is the pseudo-wells 5, 7 and 10. In the first two, organic matter of the Upper Cretaceous rocks is immature. In pseudo-well 10, the Upper Cretaceous rocks occur at the

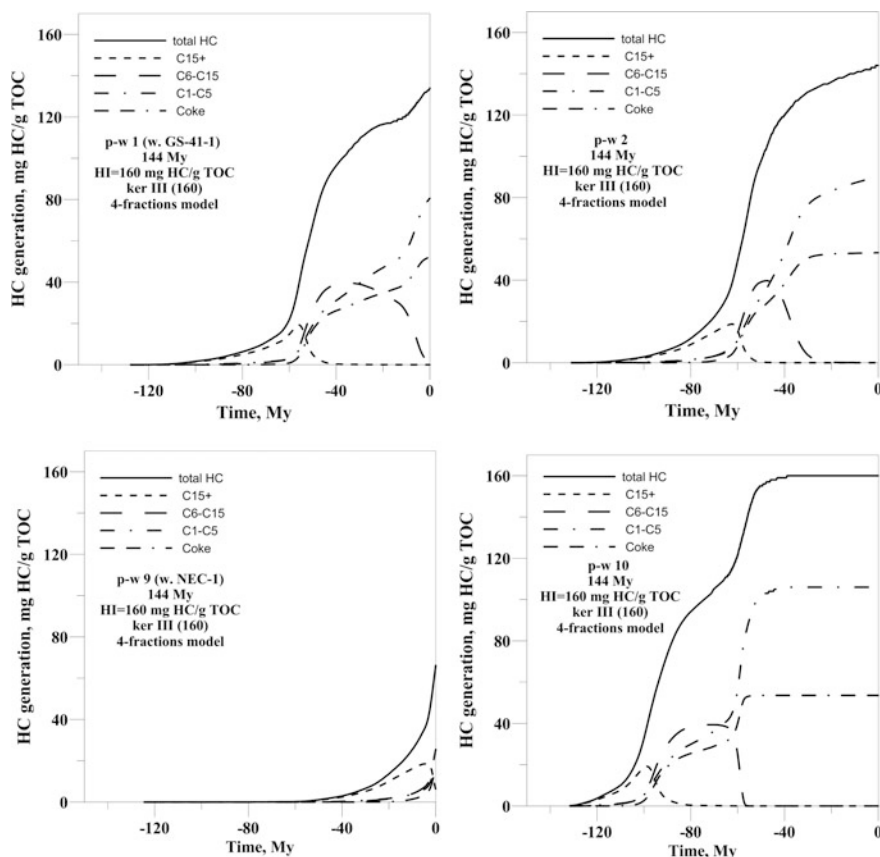


Fig. 2.18 Realization of hydrocarbon potential by the probable Lower Cretaceous source rocks of the Krishna-Godavary and Mahanadi Basins: comparison between the shallow (pseudo-wells 1 and 9 (wells GS-41-1 and NEC-1) and deep (pseudo-wells 2 and 10) areas of the eastern passive margin of India. Computations were carried out in the 4-fractions model of kerogen cracking (heavy and light oil, gas and coke)

depth more than 11 km. Their organic matter is over-mature and rocks are gas prone (Fig. 2.19; Table 2.4).

Realization of hydrocarbon potential of the Upper Paleocene source rocks is shown in Tables 2.3 and 2.4 and Fig. 2.20. In pseudowell 5 (w. KB-4-1B), located on local horst, and in shallow pseudo-well 7 (w. MND-5), maturity level of organic matter of the Upper Paleocene rocks does not exceed 0.50 % and hydrocarbon generation here is negligible (Tables 2.3 and 2.4). In pseudo-wells 1 (w. GS-41) and 3 (w. GS-5-1), located within the deep aulacagen in the region with high modern heat flow, and also in pseudo-wells 2, 4, 6, 8, 9 (w. NEC-1) maturity level ranges from 0.7 to 0.8 % and the Upper Paleocene rocks generate predominantly heavy oil. In the pseudo-well 10, these rocks are buried up to depth of 8000 m due

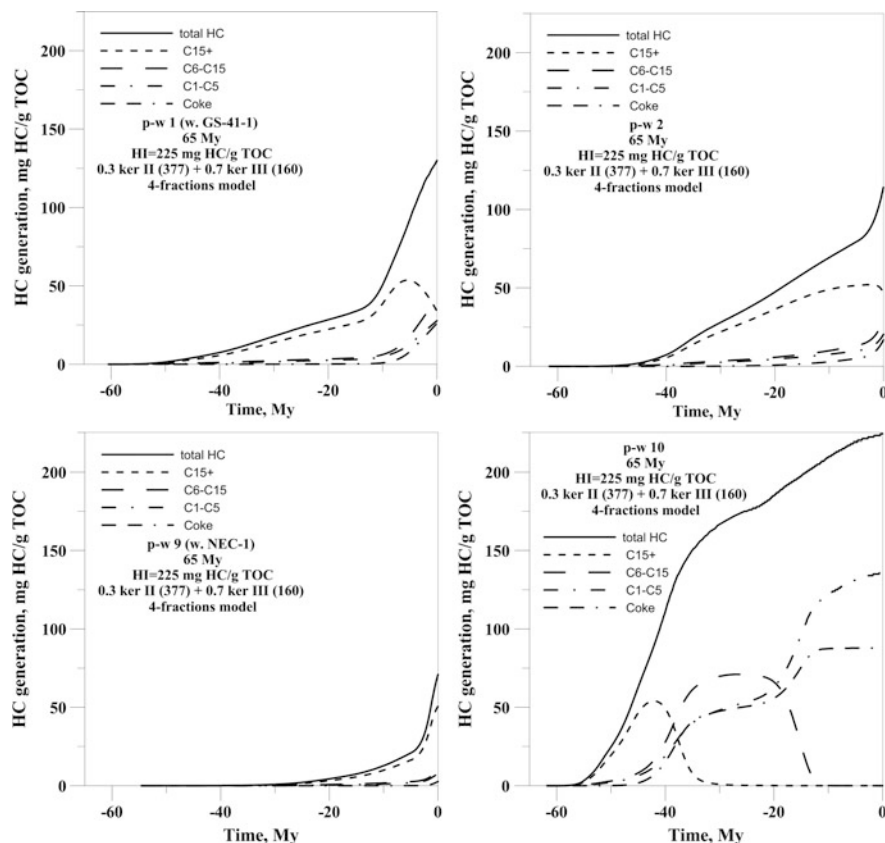


Fig. 2.19 Realization of hydrocarbon potential by probable Upper Cretaceous source rocks of the Krishna-Godavary and Mahanadi Basins: comparison between the shallow (pseudo-wells 1 and 9 (wells GS-41-1 and NEC-1)) and deep (pseudo-wells 2 and 10) areas of the eastern passive margin of India. Computations were carried out in the 4-fractions model of kerogen cracking (heavy and light oil, gas and coke)

to fan sediments of the Gang River and are gas prone at present time. However, it is possible that these rocks have generated significant volume of light oil that could migrate into upper horizons and thus avoid secondary cracking in matrix of the source rocks. Figure 2.20 shows that this possibility is quite likely in the sedimentary section of the pseudo-well 10, because the destruction of light oil remaining in the matrix of the source rocks of the Upper Paleocene, took place relatively recently, in the last 5–8 million years.

Hydrocarbon generation by the Eocene and Oligocene probable source rocks is very limited in all considered areas of the shallow and deep offshore due to low maturity level of organic matter in these rocks that does not exceed 0.70 % (Tables 2.3 and 2.4). The exception is again the area of pseudo-well 10, where avalanche sedimentation from the fan of the Gang River buried the Oligocene and

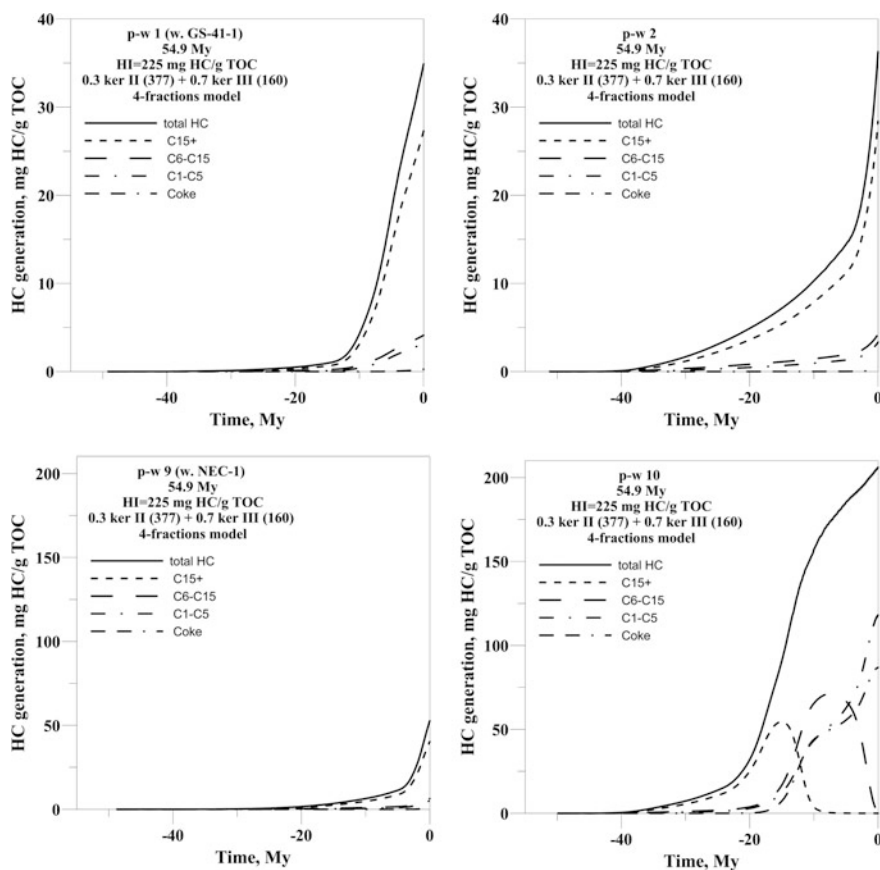


Fig. 2.20 Realization of hydrocarbon potential by probable Upper Paleocene source rocks of the Krishna-Godavary and Mahanadi Basins: comparison between the shallow (pseudo-wells 1 and 9 (wells GS-41-1 and NEC-1)) and deep (pseudo-wells 2 and 10) areas of the eastern passive margin of India. Computations were carried out in the 4-fractions model of kerogen cracking (heavy and light oil, gas and coke)

Eocene rocks at depth more 6 km and increased maturity level up to 1.1 % (Table 2.4). Table 2.4 and Fig. 2.21 show that the rocks of the Upper Eocene with kerogen of type III can generate light oil and gas, whereas the Upper Oligocene rocks with admixture of kerogen of type II generate more light oil than gas.

As a whole, Tables 2.3 and 2.4 and Figs. 2.18, 2.19, 2.20 and 2.21 demonstrate great variations in hydrocarbon generation and maturity level of probable source rocks depending on the age of formation and position of the area under study within the offshore of the Eastern continental margin of India.

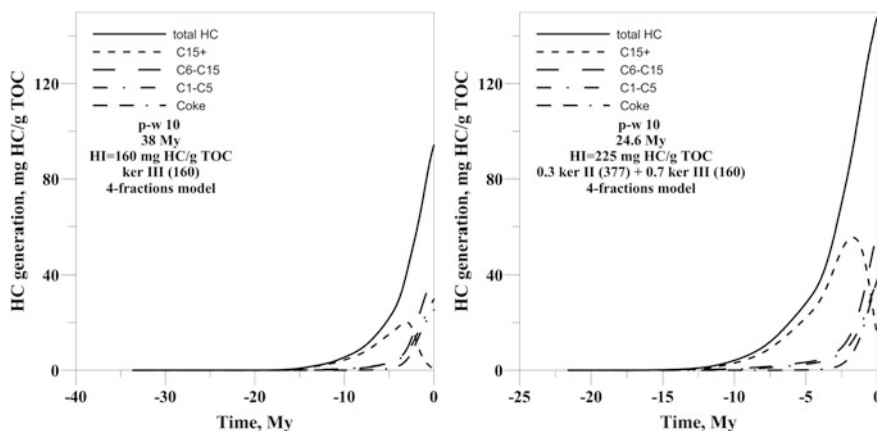


Fig. 2.21 Realization of hydrocarbon potential by the Upper Eocene and Upper Oligocene probable source rocks of the pseudo-well 10 in deep offshore of the Mahanadi Basin. Computations were carried out in the 4-fractions model of kerogen cracking (heavy and light oil, gas and coke)

2.5 Conclusion

Analysis of the basin tectonic subsidence suggests that the amplitude of the lithosphere stretching increases from $\beta = 1.03$ –1.3 in shallow-water offshore to $\beta = 1.7$ –2.9 in the deep-water offshore. As a result, the crustal thickness in the deep-water area reduced from initial value of 40 km to 25–29 km at present time (including rather thick sedimentary cover). At the same time, the sea depth increased from 50–100 m to 2–3 km. The degree of the lithosphere stretching and also the distance of the studied area from the fan of Gang River are the main factors caused the difference in burial, thermal and maturation histories of sedimentary sections in the shallow and deep-water offshore. The modeling suggests that maturity level of organic matter increases considerably toward the ocean together with the burial depth of rocks. Intensive sedimentation from the river Ganges in the Miocene-Pliocene led to considerable subsiding of “oil window” in the Krishna-Godavary and Mahanadi Basins. The rocks within the “oil window” are younger in the deep-water shelf.

References

1. Biswas SK (2012) Status of petroleum exploration in India. *Proc Indian Nat Sci Acad* 78 (3):475–494
2. Radhakrishna M, Rao SG, Nayak S, Bastia R, Twinkle D (2012) Early Cretaceous fracture zones in the Bay of Bengal and their tectonic implications: constraints from multi-channel seismic reflection and potential field data. *Tectonophysics* 522–523:187–197

3. Swamy KV, Radhakrishna Murthy IV, Krishna KS, Murthy KSR, Subrahmanyam AS, Malleswara Rao MM (2009) Magnetic anomalies of offshore Krishna–Godavari basin, eastern continental margin of India. *J Earth Syst Sci* 118(4):405–412
4. Lal NK, Siawal A, Kaul AK (2009) Evolution of east coast of India—a plate tectonic reconstruction. *J Geol Soc India* 73(February):249–260
5. Smith AG, Hallam A (1970) The fit of southern continents. *Nature* 225:139–144
6. Husain R, Mitra T, Gupta RP, Trivedi KB, Glosch A, Baghei SPS (2000) Opening of the East Coast of India vis-a-vis development of cretaceous petroleum systems. *Petroleum geochemistry and exploration in the Afro-Asian region*. In: 5-th International conference and exhibition, New Delhi, pp 535–540, 25–27 Nov
7. Acharyya SK (2000) Comment on “crustal structure based on gravity-magnetic modelling constrained from seismic studies under Lambert Rift, Antractica and Godavari and Mahanadi rifts, India and their interrelation ship” by D.C. Mishra. *Earth Planet Sci Lett* 179:595–598
8. Ramachandran K, Rabur V, Beherea BK, Harinarayana T (2013) Source rock analysis, thermal maturation and hydrocarbon generation using Rock-Eval pyrolysis in parts of Krishna-Godavary basin, India: a case study. *J Petrol Explor Prod Technol* 3:11–20. doi:[10.1007/s13202-012-0041-y](https://doi.org/10.1007/s13202-012-0041-y)
9. Ramana MV, Nair RR, Sarma KVLNS, Ramprasad T, Krishna KS, D’cruz M, Subramanyam C, John P, Subramanyam AS, Chandrashekhar DV (1994) Mesozoic anomalies in the Bay of Bengal. *Earth Planet Sci Lett* 121:469–475
10. Rao GS, Radhakrishna M (2014) Crustal structure and nature of emplacement of the 85°E Ridge in the Mahanadi offshore based on constrained potential field modeling: implications for intraplate plume emplaced volcanism. *J Asian Earth Sci* 85:80–96
11. Curray JR, Emmel FJ, Moore DG, Russel WR (1982) Structure, tectonics, and geological history of the northeastern Indian Ocean. In: Nairn AE, Stehli FG (eds) *The ocean basins and margins, the Indian Ocean*, vol 6, pp 399–450, Plenum, New York
12. Gupta RP, Husain R, Maurya SN, Venkataramatah V, Rawat S (1999) Deliberate search for subtle traps within Raghavapuram Shale: agenda for future exploration in West Godavary subbasin, Krishna-Godavary Basin. In: *Proceedings of workshop on integrated exploration for subtle and stratigraphic traps*, Dehradun, ONGC Bulletin, vol 36, Issue 1, pp 27–37
13. Gaina C, Muller RD, Brown B, Ishihara T (2003) Microcontinental formation around Australia. In: Hillis Rand Muller RD (eds) *The evolution and dynamics of the Australian plate*. Joint Geological Society of Australia. *America Special Paper*, vol 22, pp 399–410
14. Radhakrishna M, Twinkle D, Nayak S, Bastia R, Rao SG (2012) Crustal structure and rift architecture across the Krishnae Godavari basin in the central Eastern Continental Margin of India based on analysis of gravity and seismic data. *Mar Pet Geol* 37:129–146
15. Krishna KS, Michael L, Bhattacharyya R, Majumdar TJ (2009) Geoid and gravity anomaly data of conjugate regions of Bay of Bengal and Enderby Basin—new constraints on breakup and early spreading history between India and Antarctica. *J Geophys Res* 114(B03102):21. doi:[10.1029/2008JB005808](https://doi.org/10.1029/2008JB005808)
16. Ramana MV, Subramanyam V, Chaubey AK, Ramprasad T, Sarma KVLNS, Krishna KS, Mariadesa, Murty GPS, Subramanyam C (1997) Structure and origin of 85°E ridge. *J Geophys Res* 102(B8):17995–18012
17. Veevers JJ, Tewari RC (1995) Gondwana master basin of peninsular India between Tethys and the Gondwana province of Pangea. *Geol Soc Am Mem* 187:1–73
18. Gupta SK (2006) Basin architecture and petroleum system of Krishna Godavari basin, east coast of India. *Lead Edge* 25:830–837. doi:[10.1190/1.2221360](https://doi.org/10.1190/1.2221360)
19. Ramachandran K, Babu V, Behera BK, Harinarayana T (2013) Source rock analysis, thermal maturation and hydrocarbon generation using Rock-Eval pyrolysis in parts of Krishna-Godavari basin, India: a case study. *J Petrol Explor Prod Technol* 3:11–20. doi:[10.1007/s13202-012-0041-y](https://doi.org/10.1007/s13202-012-0041-y)

20. Kaila KL, Murty PRK, Rao VK, Venkateswarlu N (2005) Deep seismic sounding in the Godavari Graben and Godavari (coastal) basin. *India Tectonophys* 173(1):307–317
21. Mazumdar A, Kocherlal M, Carvalho MA, Peketi A, Joshi RK, Mahalaxmi P, Joao HM, Jisha R (2015) Geochemical characterization of the Krishna-Godavari and Mahanadi offshore basin (Bay of Bengal) sediments: a comparative study of provenance. *Mar Pet Geol* 60:18–33
22. Gupta MI, Sharma SR, Sundar A, Singh SB (1987) Geothermal studies in the Hyderabad granitic region and the crustal thermal structure of the Southern Indian shield. *Tectonophysics* 140:257–264
23. Gupta MI, Sundar A, Sharma SR (1991) Heat flow and heat generation in the Archaean Dharwar cratons and implications for the Southern Indian shield geotherm and lithospheric thickness. *Tectonophysics* 144:107–122
24. Negi IG, Panday OP, Agrawal PK (1986) Super-mobility of hot Indian lithosphere. *Tectonophysics* 131:147–156
25. Frakes LA (1979) *Climates throughout geological time*. Elsevier, Amsterdam, pp 1–310
26. Ramani KKV, Naidu BD, Giridhar M (2000) Reassessment of hydrocarbon potential of Cauvery Basin, India—A quantitative genetic model approach. *Petroleum geochemistry and exploration in the Afro-Asian region*. In: 5-th international conference and exhibition, New Delhi, pp 509–515, 25–27 Nov
27. Atlas of heat flow map of India (1991) Government of India, Delhi 65
28. Gupta ML, Sharma SR, Rao VK (2014) Conductive heat flow in the Godavari sub-basin (Pranhita-Godavari valley), Indian shield and its significance. *J Ind Geophys Union* 18(3): 394–404
29. Pytte M, Reynolds RC (1989) The thermal transformation of smectite to illite. In: Naeser ND, Mculok TH (eds) *Thermal history of sedimentary basins*. Springer, pp 132–140
30. Elliott WC, Aronson JL, Matisoff G, Gautier DL (1991) Kinetics of the smectite-to-illite transformation in the Denver Basin: clay minerals, K-Ar data, and mathematical model results. *AAPG Bull* 75:436–452
31. Huang WL, Longo JM, Pevear DR (1993) An experimentally derived kinetic model for smectite-to-illite conversion and its use as a geothermometer. *Clay Clay Miner* 41(2):163–177
32. Vasseur G, Velde B (1993) A kinetic interpretation of the smectite-to-illite transformation. In: Dore AG (ed) *Basin modeling and applications*, NPF Special Publication, vol 3, pp 173–184
33. Velde B, Vasseur G (1992) Estimation of the diagenetic smectite to illite transformation in time-temperature space. *Am Miner* 77:967–976
34. Vasseur G, Brigand F, Demongodin L (1995) Thermal conductivity estimation in sedimentary basins. *Tectonophysics* 244(1–3):167–174
35. Hunner AT (2006) Smectite to illite transformation relevance to pore pressure in the subsurface. Thesis (Internet)
36. Pande DK, Singh RR, Chandra K (2008) Source rocks in deep water depositional systems of east and west coasts of India. In: 2008 AAPG annual convention and exhibition, April 20–23, 2008, San Antonio. Search and Discovery Article #10169 (2008) Posted October 24
37. Mishra PK, Chatter TK (1995) Paleo-environmental significance of petroleum source rock deposition in the Krishna-Godavari, Cauvery and Andaman basins: an integrated approach through the paleontological and geochemical parameters from selected case studies. In: *Proceedings of PETROTECH-95*, New Delhi, Technology Trends in Petroleum Industry
38. Rangarajy MK, Agrawal A, Prabhakar KN (1993) Tectono-stratigraphy, structural style, evolutionary model and hydrocarbon habitat, Cauvery and Palar basins. In: Biswas SK et al (eds) *Proceedings second seminar on petroliferous basins of India*, vol 1, Indian Petroleum Publishers, Dehra Dun, 248001, India, pp 371–389
39. Espialie J, Ungerer P, Irvin I, Marquis E (1988) Primary cracking of kerogens. Experimenting and modelling C1, C2-C5, C6-C15 classes of hydrocarbons formed. *Org Geochem* 13(4–6): 893–899

40. Ungerer Ph (1993) Modeling of petroleum generation and migration. In: Bordenave ML (ed) Applied petroleum geochemistry, Technip, Paris, pp 397–442
41. Welte DH, Horsfield B, Baker DR (eds) (1997) Petroleum and basin evolution, Springer
42. Makhous M, Galushkin Y (2005) Basin analysis and modeling of the burial, thermal and maturation histories in sedimentary basins. TECHNIP, Paris
43. Galushkin Yu, Eloghbi S, Sak M (2014) Burial and thermal history modelling of the Murzuq and Ghadames Basins (Libya) using the GALO computer programme. J Petrol Geol 37(1):69–92



<http://www.springer.com/978-3-319-33881-1>

Non-standard Problems in Basin Modelling

Galushkin, Y.

2016, XIII, 268 p. 129 illus., Hardcover

ISBN: 978-3-319-33881-1